$^{13}C/^{19}F$ High-resolution solid-state NMR studies on layered carbon-fluorine compounds

Miwa Murakami [a,*], Kazuhiko Matsumoto [b], Rika Hagiwara [b], and Yoshiaki Matsuo [c]

[a]Office of Society-Academia Collaboration for Innovation, Kyoto University, Gokasho, Uji, Kyoto, 611-0011, Japan.

[b]Graduate School of Energy Science, Kyoto University, Yoshida-honmachi, Sakyo-ku, Kyoto, 606-8501, Japan.

[c]Graduate School of Engineering, University of Hyogo, 2167, Shosha, Himeji, Hyogo 671-2280, Japan.

[*] Corresponding author. E-mail: m-murakami@saci.kyoto-u.ac.jp (Miwa Murakami)
Tel: +81-774-38-4967, Fax: +81-774-38-4996

Abstract

$^{13}C/^{19}F$ high-resolution solid-state NMR was applied to examine local structures of a stage-1 layered carbon-fluorine compound ($C_{2.8}F$). Four ^{19}F (F1~F4) and two ^{13}C signals (C1 and C2) unraveled by high magnetic field (14 T) and fast magic-angle spinning (> 35 kHz) were examined by various two-dimensional correlation experiments. In addition to "through space" ^{13}C-^{19}F and ^{19}F-^{19}F dipolar correlation, which reveals distance proximity among $^{13}C/^{19}F$ spins, we examined feasibility of applying the *J* interaction for examination of "through bond" correlation. These experiments led assignment of two of the four F signals (F2 and F3) to F directly covalent bonded to sp^3 carbon and an interleaving domain for the local structure of the minor C2-F3 group among the major domain composed of C2-F2 and sp^2 carbon (C1). The other two ^{19}F signals (F1 and F4) were assigned to as CF_2 and F ions, respectively. A spectroscopic evidence for the C-F bond being the σ bond is given by the observation of a non-zero one-bond *J* value (193 ± 4 Hz) for C2-F. Further, the similar J_{CF} = 197 Hz for C-F in poly(carbon fluoride) confirmed that the so-called "semi-ionic/semi-covalent" C-F bond in $C_{2.8}F$ is actually a "standard" covalent C-F bond.

1. Introduction

Fluorination of graphite provides a variety of compounds with unique structures [1,2]. Direct fluorination of graphite with elemental fluorine at high temperatures leads to formation of layered carbon fluorides; the products are classified into fluorinated poly(carbon monofluoride) ($(CF)_n$) and poly(dicarbon monofluoride) ($(C_2F)_n$), depending on synthetic temperature (~873 K for $(CF)_n$ and ~623 K for $(C_2F)_n$), and have characteristic structures with covalent C−C and C−F bonds, as shown in Figs. 1 (a) and (b). While $(CF)_n$ is composed of single cyclohexane-like buckled sheets of sp^3-hybridized carbon atoms, $(C_2F)_n$ has two adjacent sheets bonded by covalent C-C bond along the stacking direction [3-8]. Another type of layered carbon fluorides called C_xF are prepared at lower temperature via catalytic formation of intercalation compounds. Several Lewis acidic catalysts are reported for this purpose such as HF, AsF_5, and IF_5 (AF_m) [9-17]. Reaction of graphite and these Lewis acids first gives intercalation compounds in the form of $C_x(AF_{m+1})$, and further fluorination along with elimination of AF_m results in formation of C_xF.

The C_xF-type compounds are considered to possess non-saturated C−C bond and different C−F bond, which was previously called “semi-ionic” (or “semi-covalent"), from those in $(CF)_n$ and $(C_2F)_n$. A neutron diffraction study for C_xF with stage-1 structures (x = 2.47, 2.84, 3.61) revealed that the C-F bond in C_xF was essentially covalent with the C-F bond length of 0.140 nm, and the graphite sheets are buckled at the sp^3-hybridized carbon atoms bound to fluorine atoms as shown in Fig. 1 (c) [18]. Such modification was attributed to hyperconjugation involving the C−F and C−C bonds. The observed higher-frequency shift of the ^{19}F NMR chemical shift in C_xF compared to those in covalent $(CF)_n$ and $(C_2F)_n$ was ascribed to weakening of covalency

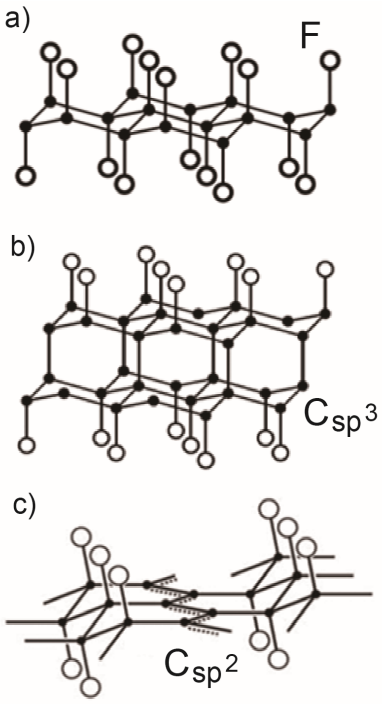

Figure 1. Molecular structures of $(CF)_n$ (a), $(C_2F)_n$ (b), and C_xF (c).

by hyperconjugation between the C-F group and the adjacent sp^2 carbons in nonsaturated C_xF [19]. Further, solid-state NMR measurements for $C_{2.5}F$ and obtained a similar C-F bond length also supported that the C-F bonding in this material is essentially covalent, and the so-called "semi-ionic" (or “semi-covalent") should be rather denoted as "weakened covalent" C-F bonding [20].

In the course of our recent efforts [21] to develop a so-called fluoride-shuttle battery (FSB) [22], we gained renewed interest in C_xF. It has been studied for the cathode of lithium primary battery, and it delivered high capacity with high operating voltages [23-25]. This means that it contains a large amount of electrochemically active fluorine atoms. Moreover, it shows not only relatively high electrical, but also fluoride

ion conductivities [26]. These properties are favorable for the use of it as a cathode active material of FSB.

In application of C_xF as materials for a FSB, one has to characterize the chemical nature of the C-F bond in the C_xF material as it has been shown that the C-F bond in a carbon/fluoride system can vary from covalent to ionic one thorough what may be called as semi-ionic/semi-covalent bonding [27]. In this work, we apply high-resolution solid-state NMR to examine $C_{2.8}F$. High resolution achieved by high static magnetic field (14 T) and fast magic-angle spinning (35 and 60 kHz) reveals four distinct ^{19}F signals, two of whose assignment have not been addressed. Various experiments including two-dimensional (2D) $^{19}F/^{19}F$ and $^{13}C/^{19}F$ dipolar correlation experiments were applied for signal assignment and structural determination. In addition to $^{19}F/^{19}F$ and $^{13}C/^{19}F$ "through-space" dipolar interactions to examine proximities among the ^{13}C and ^{19}F sites, we also used the ^{13}C -^{19}F "through-bond" spin-spin coupling (*J*) interaction, which is useful not only for signal assignment but also for examination of covalency or the s-character of the C-F bond. Roughly speaking, it has been suggested that the one-bond ^{19}F-^{13}C *J* coupling (J_{CF}) among a series of organic compounds reflects the relative amount of s-character in the carbon orbital that is used in bonding to fluorine; the more s-character, the larger the C-F coupling constant [28]. It is thus of interest to compare J_{CF} values in C_xF and its covalent counterpart $(CF)_n$. Though the *J* interaction is quite useful for signal assignment as well as examination of the nature of the chemical bond, it has not yet been utilized in solid-state NMR of a carbon/fluoride system. This may be due to apparent ^{13}C linewidth being much broader than the J_{CF} coupling (160~285 Hz for the direct C-F bond [28]) obscures the *J* splitting. We show in this work that by application of proper pulse sequences, one can remove

inhomogeneous broadening due to variation of the local structure and obtain the J_{CF} coupling constant. Furthermore, we show that ^{13}C-^{19}F heteronuclear correlation experiment based on the *J* interaction (*J*-HMQC) can also be applicable for C_xF.

2. Experimental

2.1 Sample preparation

Volatile materials were handled in a vacuum line constructed of stainless steel and PFA (tetrafluoroethylene-perfluoroalkylvinylether-copolymer). Nonvolatile materials were handled under a dry Ar atmosphere in a glovebox. Graphite powder (Union Carbide, SP-1 grade, purity 99.4 %, average particle diameter 0.1 mm) and elemental fluorine (Daikin Industries, purity 99.7 %) were used as supplied. Anhydrous HF (Daikin Industries, purity 99.98 %) was dried over K_2NiF_6 prior to use. The C_xF sample was prepared by reaction of graphite, HF, and fluorine gas. The starting graphite powder was loaded in a PFA tube, and 0.10 MPa of HF vapor was introduced onto it. Then, fluorine gas was introduced up to 0.20 MPa. After agitation for 24 hr, the pressure of gas phase was reduced by reaction, and fluorine gas was introduced again up to 0.20 MPa. After further reaction for 7 hr, the volatiles were pumped off at 298 K for 1 hr and at 373 K for 12 hr.

The fluorine contents of the obtained samples were estimated to be C/F = 2.8 by the elemental analysis of carbon and fluorine at the Center for Elemental Microanalysis of Kyoto University with the aid of CHN corder and oxygen flask method. We shall hereafter refer the C_xF sample thus prepared to as $C_{2.8}F$. The Rama, X-ray diffraction, and X-ray photoelectron spectra of $C_{2.8}F$ are given in the Supplementary Data.

The $(CF)_n$ sample was prepared by direct fluorination of graphite at 873 K. The starting graphite powder was loaded in a nickel tube reactor under a dry Ar atmosphere, and fluorine gas was flowed on it at 873 K for 4 hr, followed by further fluorination at 873 K for 20 hr under a fluorine atmosphere at 0.12 MPa. The C/F ratio of the resulting product was determined to be 1.1, and the product is called $(CF)_n$ hereafter.

2.2 NMR measurement

Most of the NMR measurements were made using a JEOL ECA600 NMR spectrometer with a triply-tuned MAS probe (Agilent Technologies Inc.) for a 1.6 mm rotor at 14 T. The ^{19}F MAS spectrum observed under the MAS spinning frequency (ν_R) of 60 kHz was taken by using an Agilent DD2 600 MHz NMR spectrometer with a triply-tuned MAS probe (Agilent Technologies Inc.) for a 1.2 mm rotor. The resonance frequencies for ^{19}F and ^{13}C were 564 MHz and 151 MHz, respectively. The ^{19}F chemical shifts were calibrated in ppm relative to CCl_3F adopting the ^{19}F chemical shift for LiF (-203 ppm [29]) as an external reference. The ^{13}C chemical shifts were calibrated in ppm relative to tetramethylsilane (TMS) by adopting the ^{13}C chemical shift for the methine carbon nuclei of solid adamantane (29.5 ppm) as an external reference. The temperature-calibration experiment was done using ^{207}Pb NMR of $Pb(NO_3)_2$ [30]. The one-dimensional (1D) ^{19}F MAS spectra were taken by using a single-pulse method with the spin echo. The 1D ^{13}C MAS NMR spectra were observed by using a single-pulse method or a ^{19}F to ^{13}C cross-polarization (CP) method with the conventional constant-amplitude CP pulse sequence. The ^{19}F rf amplitudes (ν_{1F}) used in CP was ca. 75 kHz and that for ^{13}C (ν_{1C}) was ca. 40 kHz to satisfy the n = 1 Hartman-Hahn condition under MAS [31], that is, $\nu_{1F} = \nu_{1C} + n\,\nu_R$. Except for the ^{19}F MAS NMR spectrum given in Fig. 2 (a) (see below), all MAS experiments have been done under ν_R = 35 kHz.

To appreciate the ^{13}C-^{19}F J coupling, one can not apply ^{19}F dipolar decoupling, because it also decouples the J interaction. We found that, under ν_R = 35 kHz, ^{19}F decoupling is not necessary as no ^{13}C line narrowing was appreciable under ^{19}F

decoupling using the XiX scheme [32] with amplitude of ca. 80 kHz. Hence, the ^{13}C spectra in this work were obtained without ^{19}F decoupling. The inefficiency of decoupling is attributable efficient averaging of ^{13}C-^{19}F dipolar interaction by fast MAS with ν_R = 35 kHz. In fact, we often observed line broadening instead of line narrowing caused by application of ^{19}F decoupling, which is ascribable to rotary resonance recoupling [33].

For signal assignment as well as structural examination, we applied various two-dimensional (2D) experiments [34], namely, ^{13}C-^{19}F heteronuclear correlation experiment using CP (CP-HETCOR), 2D ^{19}F-^{19}F exchange NMR, and 2D ^{13}C-^{19}F *J*-HMQC experiment (the HMQC sequence is illustrated in the Supplementary Data). The ^{13}C-^{19}F *J* coupling constant was obtained by using the single-quantum *J*-filter (*J*-1QF) experiment [35, 36], which is described more precisely in the Supplementary Data. Further, the ^{19}F spin-lattice relaxation times (T_1) under MAS were measured by using the conventional saturation-recovery method with the recovery data being fitted to a single exponential curve.

Here we would like to point out that we use "high-frequency shift" and "low-frequency shift" instead of "low-field shift" and "high-field shift". The latter pair is suitable for ancient continuous-wave (CW) NMR, in which magnetic field is swept between low to high fields, but not for current FT-NMR.

3. Results

Fig. 2 shows the ^{19}F MAS spectra of $C_{2.8}F$ (a, b) and $(CF)_n$ (c) taken at the MAS spinning frequency (ν_R) of 60 kHz (a) and 35 kHz (b,c). We temporarily labeled the four signal components (F1~F4) in $C_{2.8}F$ as indicated in Fig. 2(a). The positions of two spinning sidebands of F2 are indicated by the vertical dashed lines in Figs. 2 (a) and (b).

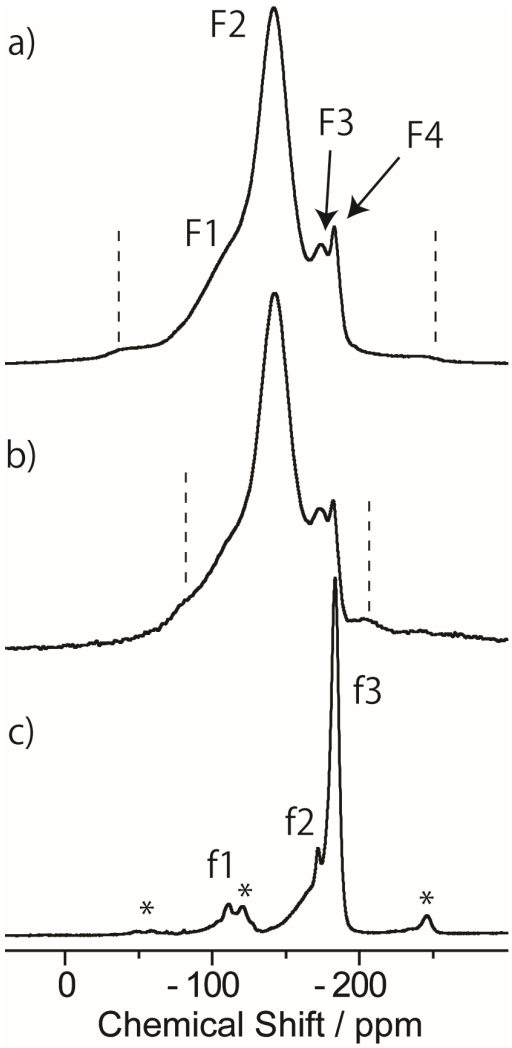

Figure 2. ^{19}F MAS spectra of $C_{2.8}F$ (a, b) and $(CF)_n$ (c) taken with ν_R = 60 kHz (a) and 35 kHz (b, c). The positions of the spinning sidebands of F2 are designated by the vertical dashed lines in (a) and (b). The peaks marked by * in (c) are the spinning sidebands.

Among anisotropic spin interactions for $I = 1/2$, which bring spinning sideband, it was shown that the homonuclear ^{19}F-^{19}F dipolar interaction is well averaged by MAS even with ν_R = 12 kHz [20]. Hence the spinning sidebands are attributable to the chemical-shift anisotropy of F2 manifested itself by the application of high magnetic field of 14 T. Fig. 2 indicates that the spinning sidebands of F2 do not overlap significantly with the other signals. Hence, we adopted the 1.6 mm rotor for 35 kHz MAS in the experiments described below.

In $(CF)_n$ (Fig. 2(c)), the f1 signal at -111 ppm and f3 at -183 ppm are assigned to be CF_2 and CF, respectively, according to those reported for $(CF)_n$ at -109.5 ppm and -180.5 ppm [37], and -116 ppm and -187 ppm [38]. The signals marked by asterisks in Fig. 2(c) are the spinning sidebands of f3 as confirmed by observing ν_R dependence given in the Supplementary Material. The small signal intensity for f1 indicates that the relative amount of the sheet edges and other defected structures are small for the starting graphite material. This will also be confirmed by the ^{13}C spectrum given below. The small signal (f2) at -172 ppm may be the same one labeled as F3 in $C_{2.8}F$. Further a broad signal component at around -160 ppm is discernible, which may be ascribable to C-F with distorted structures.

In Fig. 3 (b), we showed the results of lineshape analysis for the ^{19}F spectrum (the black line in Fig. 3(a)) after subtraction of background signals (the red line in Fig. 3 (a)) ascribed to fluoropolymers used in the NMR probe. The spectrum was successfully fitted to the sum of six Lorentz lineshapes representing F1 to F4 signals and two spinning sidebands of F2. The chemical shift values obtained are F1: -106 ppm, F2: -143 ppm, F3: -173 ppm, and F4: -182 ppm, and the intensity ratio is F1:F2:F3:F4 = 0.12:1.0:0.11:0.07. The chemical shift for F2 is consistent with that reported for F with

sp^3 carbon in $C_{2.5}F$ (-147 ppm) [20]. Experimental results for ^{19}F signal assignment are described after brief examination of the ^{13}C MAS spectra (Fig. 4).

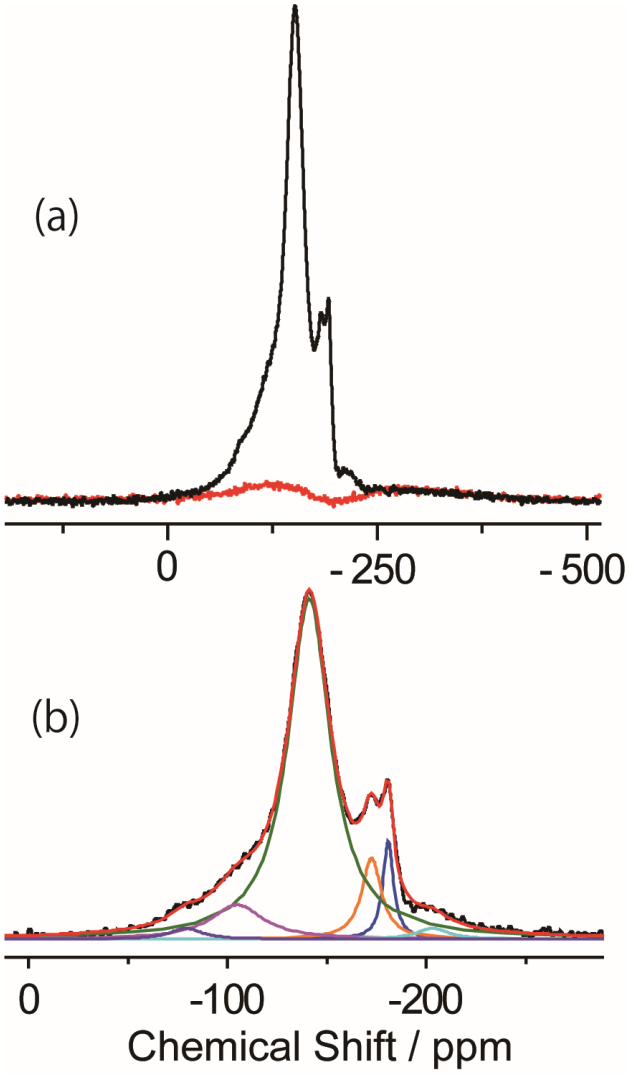

Figure 3. (a) ^{19}F background signals (the red line) are plotted with the observed ^{19}F spectrum of $C_{2.8}F$ (the black line; the same one in Fig. 2 (b)). The background signals were subtracted from the observed spectrum, and the remaining spectrum (the black line) was fitted to the sum (the red line) of six Lorentz lineshapes (the other color lines).

The ^{13}C MAS spectra in Figs. 4 (a) to (c) are of $C_{2.8}F$ and that in Fig. 4 (d) is of $(CF)_n$. The red dotted line is drawn at 111 ppm to designate the reported chemical shift

for CF_2 (*vide infra*). In the ^{13}C MAS spectrum taken by using the single-pulse experiment (Fig. 4 (a)) and that by using ^{19}F to ^{13}C CP (Fig. 4 (b)), two signals referred to as C1 and C2 hereafter are observed at 129 ppm and 83 ppm, respectively. Again these shifts are consistent with those observed for $C_{2.5}F$ (128 ppm and 82 ppm), which are assigned to as non-fluorinated sp^2 and fluorinated sp^3 carbons, respectively [20]. The

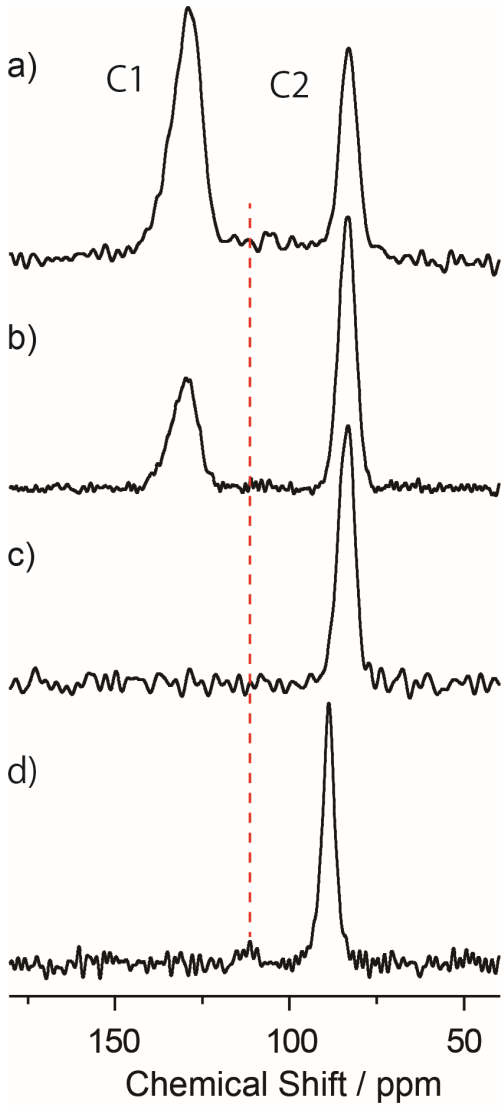

Figure 4. ^{13}C MAS spectra of $C_{2.8}F$ (a-c) and $(CF)_n$ (d). The spectrum (a) was taken with a single pulse, and those (b) and (d) were by using ^{19}F to ^{13}C CP. The spectrum (c) is the single-quantum *J*-filtered spectrum taken with the *J* evolution time of τ = 2.28 ms.

single-quantum (1Q) J_{CF} filtered spectrum shown in Fig. 4 (c) will be touched upon afterward. Analysis of the ^{13}C-^{19}F dipolar oscillation for the C1 and C2 signals during the contact time of CP at the n = 1 Hartman-Hahn condition under MAS [39] was done, and the results are given in Supplementary Material. From the observed ^{13}C-^{19}F dipolar splitting of 7.4 kHz, the C-F distance between C2 and nearest F was estimated to be 0.14 nm, which is consistent to that observed for $C_{2.5}F$ by [20] and neutron diffraction [18]. Dipolar splitting was not appreciable for C1, indicating a much longer C1-F distance, which confirms the above assignment.

Two ^{13}C signals are observed for $(CF)_n$ (Fig. 4 (d)); one at ca. 110 ppm and the other at 89 ppm, which are consistent with those reported for $(CF)_n$; 111 ppm (CF_2) and 88 ppm (CF) in Ref. [37] and 111 ppm (CF_2) and 89 ppm (CF) in Ref. [38]. Again the small CF_2 signal at ca. 110 ppm indicates less edges/defects in the starting graphite material. As $C_{2.8}F$ was obtained from the same graphite material, we expect that the amount of edges/defects is also small in $C_{2.8}F$, and in fact, the CF_2 signal, which would appear at around 110 ppm, is not appreciable for $C_{2.8}F$ (Figs. 4 (a) to (c)). This will be discussed afterward.

So far, we mainly confirmed the assignments for signals F2, f1, f2, C1, and C2 reported previously. Next we proceed to examine distance proximity among the four fluorine sites (F1~F4) and the two carbon sites (C1 and C2) for $C_{2.8}F$ by using 2D CP-HETCOR. Fig. 5 (a) shows the observed 2D CP-HETCOR contour spectrum taken with the CP contact time of 1.2 ms, showing that both C1 and C2 are in close proximity to F2. While for F3, the C1-F3 cross peak is much smaller than that for C2-F3, indicating a longer distance between F3 and C1. The ^{19}F cross-section spectrum at C2 (designated by the vertical dashed line in Fig. 5 (a)) is shown in Fig. 5 (c) to compare

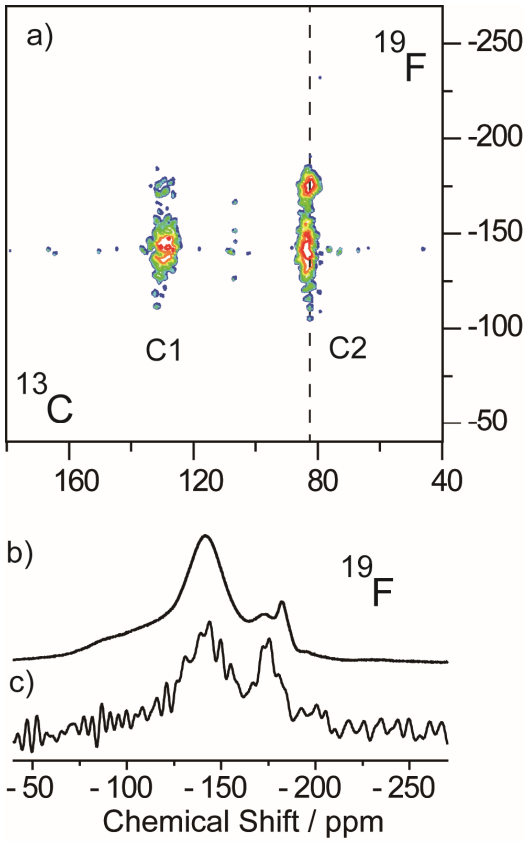

Figure 5. 2D heteronuclear correlation (HETCOR) spectrum using CP (a) together with the 1D ^{19}F MAS spectrum (b) and the ^{19}F cross-section spectrum at the C2 signal (c) designated by the vertical dashed line in (a). The CP contact time was 1.2 ms.

with the 1D ^{19}F MAS spectrum in Fig. 5 (b) (the same one in Fig. 2 (b)). Apparently, F4 has no dipolar correlation with ^{13}C, while other F1~F3 have. The F4 signal at -182 ppm is thus assigned to F^- associated with delocalized positive charge on sp^2 carbon region in the carbon layer. Slightly different chemical shift (-190 ppm) was reported in $C_{2.5}F$ [20]. This assignment of F4 is further confirmed by examination of temperature dependence of the ^{19}F lineshape and T_1 (*vide infra*). Lastly, we would like to point out that the relatively larger cross peak for C2-F3 than that for C2-F2 does not necessarily mean a shorter

C2-F3 distance, because the larger C2-F3 signal can be attributable to concentration of the F3 signal onto C2, while the F2 signal is divided into C1 and C2.

Distance proximities among the four F sites were examined by 2D ^{19}F-^{19}F exchange NMR experiment with the mixing time of 200 ms (Fig. 6 (b)) and 500 ms (Fig. 6 (c)). Fig. 6 (a) shows the 1D ^{19}F spectrum for comparison. Those rather long mixing

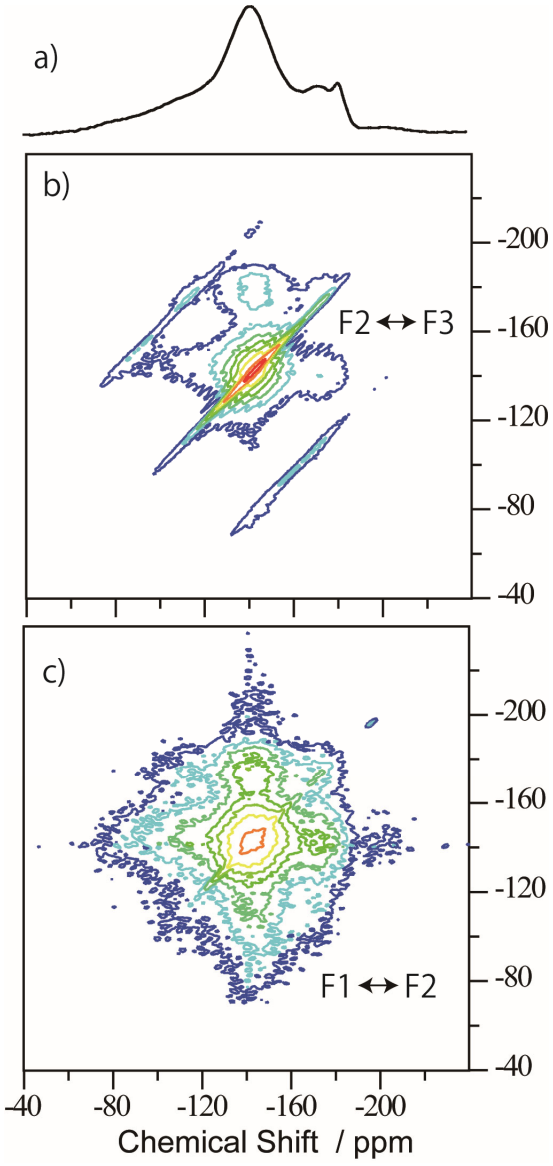

Figure 6. 2D ^{19}F-^{19}F exchange NMR spectra with the mixing time of 200 ms (b) and 500 ms (c) with the 1D ^{19}F MAS spectrum (a).

times required for ^{19}F spin exchange indicates that fast MAS with ν_R = 35 kHz reduces ^{19}F-^{19}F homonuclear dipolar interactions appreciably, and the characteristic time constant for ^{19}F-^{19}F spin-diffusion becomes ca. a hundred ms for F2 and F3. A much longer diffusion time is necessary for F2 and F3. The roughly estimated spin-diffusion time for F2 and F3 will be used in evaluation of the size of the F3 domain (Discussion 4.2).

The large cross peaks between F2 and F3 in Fig. 6 (b) indicate that F2 and F3 are in close proximity. The cross peaks between F1 and F2/F3 observed at the mixing time of 500 ms implies that F1 is rather far from F2/F3 but not isolated from the main structure of $C_{2.8}F$ composed of F2 and F3. In other words, F1 is not attributable to isolated fragmentary crystalline of carbon/fluorine compounds created by fluorination reaction. In contrast, there is no cross peak between F4 and others. This is consistent with the assignment of F4 being F^-. To further confirm this assignment of F4, we examined temperature dependence of the ^{19}F lineshape and T_1.

The ^{19}F MAS spectrum in Fig. 7 (a) was taken at 80 ˚C and that in Fig. 7 (b) at -40 ˚C. The lineshape is independent of temperature except for F4, which exhibits motional narrowing at higher temperature. Fig. 8 shows temperature dependence of ^{19}F T_1 observed for F1~F4 under MAS with ν_R = 35 kHz. As have shown in the ^{19}F-^{19}F exchange NMR (Fig. 6), fast MAS slows down ^{19}F-^{19}F spin diffusion, and its time constant becomes ca. a few hundred ms. As the T_1 values for F1-F3 are comparable to the ^{19}F-^{19}F spin-diffusion time constant, the averaging of T_1 by spin diffusion does not occur efficiently, leading to the observed individual T_1 values for F1-F3. The better degree of coincidence between the T_1 values of F2 and F3 than that between F1 and F2

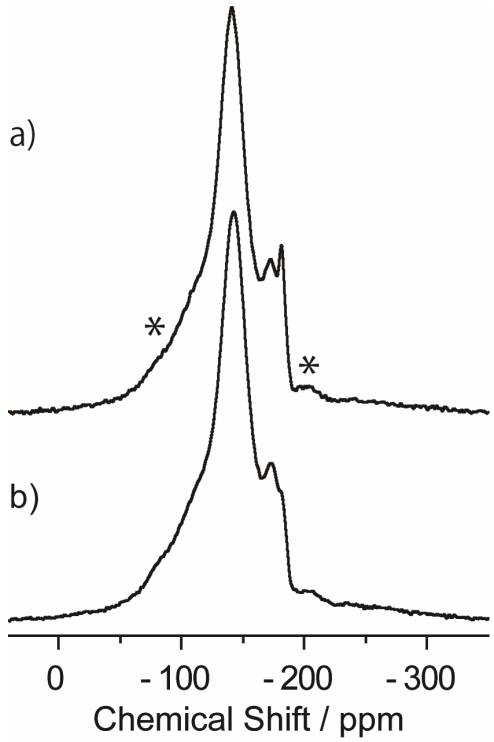

Figure 7. Temperature dependence of the ^{19}F MAS spectra taken at 60 ˚C (a) and -40 ˚C (b). The peaks marked by * in (a) are the spinning sidebands.

(or F1 and F3) is consistent with the faster ^{19}F-^{19}F transfer for the former pair found in 2D ^{19}F-^{19}F exchange NMR (Fig. 6).

The short T_1 of F4 is attributable to facile motion of F^-. From the temperature dependence, it is clear that motion of F4 governing its T_1 is in the strong-collision limit ($\omega_0\tau_c >> 1$, where ω_0 is the ^{19}F Larmor frequency at 14 T and τ_c is the correlation time of motion), and the activation energy for motion was estimated to be ca. 3.3 kJ/mol from the slope of the straight line through the data points. Though it does not lead any conclusions, we would like to point out that the activation energy is about twice of that obtained for ^{19}F in $(CF)_n$, that is, 1.7 ± 0.1 kJ/mol [37]. To conclude, no $^{19}F/^{19}F$ and $^{13}C/^{19}F$ dipolar correlation for F4 as well as the observed motional narrowing and its short T_1 lead us to assign F4 being free F^- ions.

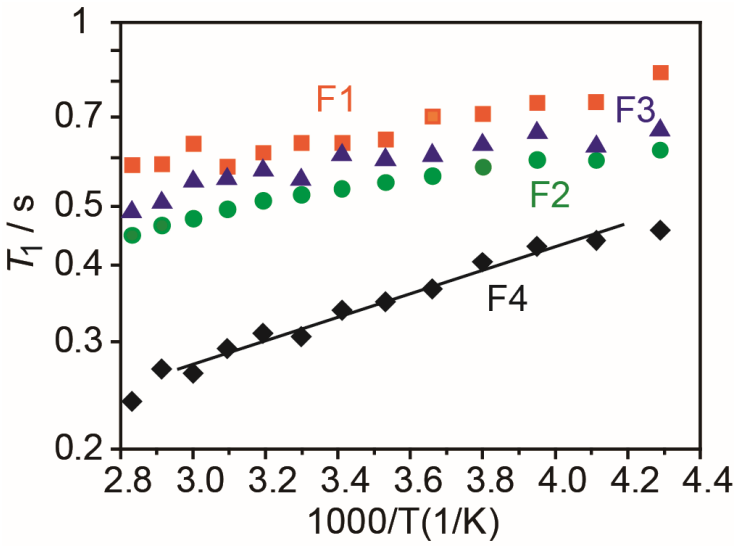

Figure 8. Temperature dependence of ^{19}F spin-lattice relaxation time (T_1) for F1 (orange squares), F2 (green circles), F3 (purple triangles), and F4 (black diamonds). The slope of the solid dark green line through the F4 data points corresponds to an activation energy of 3.3 kJ/mol.

Having described "thorough-space" dipolar correlation, which is useful but cannot be directly related to chemical bonding, we now proceed to examine the use of the J_{CF} "through-bond" coupling. In trying to obtain the J_{CF} coupling constant for C2-F, we examined various *J*-resolved methods and found that the *J*-1QF experiment [35, 36] is the most feasible.

The results of the ^{13}C observed *J*-1QF experiment are given in Fig. 9. The red circles show the observed refocusing-time (τ; defined in Fig. S5 in the Supplementary Data) dependence of the ^{13}C signal intensity of C2 in $C_{2.8}F$ and the black squares that of the CF signal in $(CF)_n$. The τ dependence is written as [35, 36]

$$I(\tau) = I_0 \sin^2(\pi J_{CF} \tau) \exp(-2\tau/T_2), \qquad (1)$$

where J_{CF} is the ^{13}C-^{19}F J coupling constant, and I_0 is the initial ^{13}C intensity. The ^{13}C spin-spin relaxation time T_2 was obtained to be 12.0 ± 0.7 ms (error is σ, hereafter) and 2.2 ± 0.1 ms for $C_{2.8}F$ and $(CF)_n$, respectively, by the independent ^{13}C spin-echo experiments (not shown). The observed intensities were then least-squares fitted to Eq. (1) by taking J_{CF} and I_0 as adjustable parameters, and the solid lines in Fig. 9 are the best-fit ones. The best-fit J_{CF} is 193 ± 4 Hz for $C_{2.8}F$ and 197 ± 7 Hz for $(CF)_n$. The larger error in the J_{CF} value for $(CF)_n$ is also ascribable to the shorter ^{13}C T_2 value in $(CF)_n$. Note here that, in the above fitting, the experimental error in the T_2 value was not propagated to the error for J. Hence, the above error values for J are slightly underestimated ones.

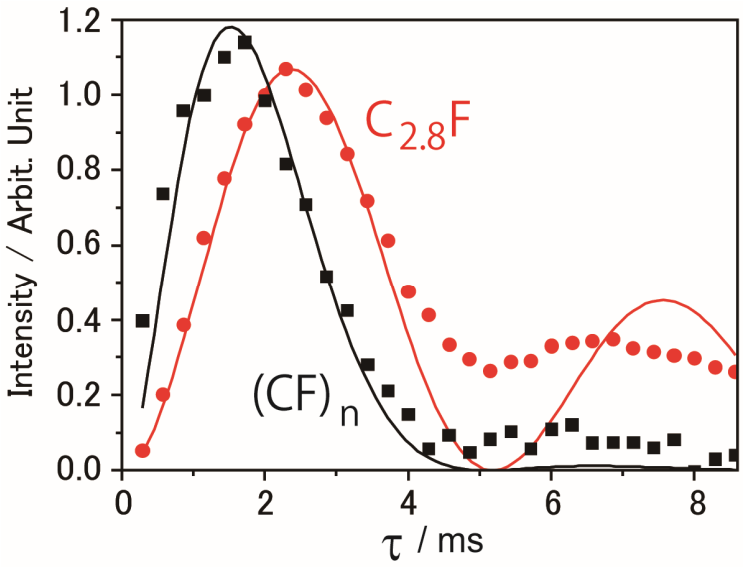

Figure 9. Refocusing time (τ) dependence of the C-F carbon (C2) signal intensity of $C_{2.8}F$ (red circles) and $(CF)_n$ (black squares) in ^{13}C-^{19}F J-1QF experiments. The solid lines were the best-fit ones as described in the text.

The deviation of the best-fit curves from the observed data at longer τ is apparent, which is attributable to dumping of *J*-oscillation due to ^{19}F T_2 not included in Eq. (1). Indeed the observed ^{19}F T_2 is very short, for example 1.8 ± 0.1 ms for $C_{2.8}F$, which makes it difficult to apply the ^{19}F observed *J*-1QF experiment. Note further that the sign of *J* cannot be determined by this experiment, which is likely to be minus [28]. In the following, we ignore the sign and write simply, for example, J_{CF} = 193 Hz. The 1D *J*-1QF spectrum at τ = 2.28 ms is shown in Fig. 4 (c), suggesting that there is no fluorine directly bonded to C1. In other words, the C1-F correlation signals in Fig. 5 are "through-space" ^{13}C-^{19}F dipolar origin.

Though the observed short ^{19}F T_2 (1.8 ± 0.1 ms) for $C_{2.8}F$ suggested difficulties of observing HMQC signals, we attempted it with the *J*-transfer time (described more precisely in Fig. S4 in the Supplementary Data) with *J* = 200 Hz, and the observed 2D *J*-HMQC spectrum is given in Fig. 10 (c) with the 1D ^{19}F spectrum (Fig. 10 (a)). As expected from the 1D *J*-1QF spectrum in Fig. 2(c), only ^{13}C-^{19}F correlation signals for C2 and F2/F3 were observed. We also obtained the HMQC spectra for *J* = 150 Hz and 500 Hz (not shown). The former gave no signals, and the latter gave the spectrum similar to that for the *J* = 200 Hz one. The loss of signal for *J* = 150 Hz is ascribed to T_2 decay of ^{19}F and ^{13}C signals. The spectrum in Fig. 10 (b) is the cross section at the C2 signal designated by the horizontal dashed line in Fig. 10 (c). By comparing with the 1D spectrum in Fig. 10 (a), we concluded that the F1 fluorine (and F4) does not form covalent bond with the C2 carbon, while both F2 and F3 form covalent bond with the C2 carbon.

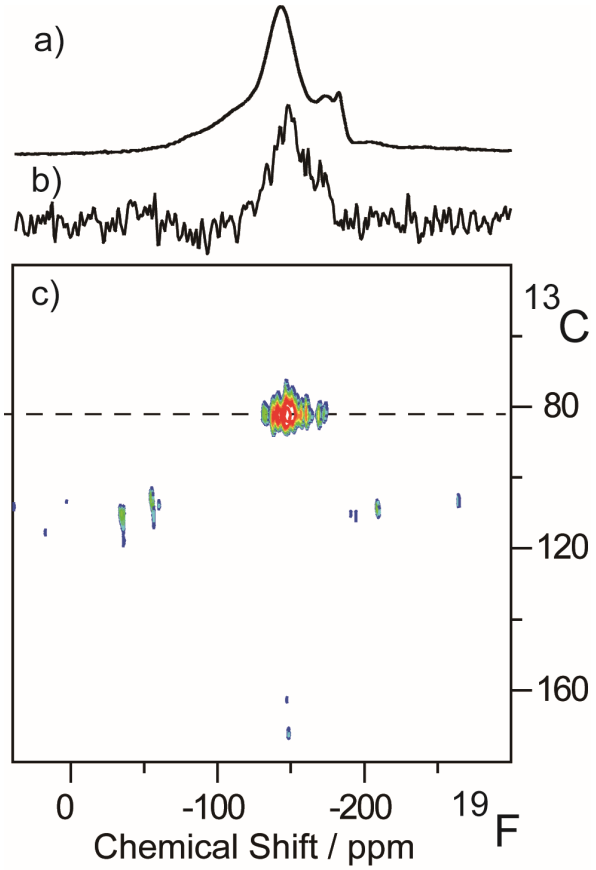

Figure 10. 1D ^{19}F MAS spectrum (a) and the ^{19}F cross-section spectrum at the C2 signal designated by the horizontal dashed line in the *J*-HMQC spectrum (c).

4. Discussion

4.1. ^{19}F signal assignment

Firstly, we discuss assignment of F1 at -106 ppm. Three possibilities may be invoked. The first one, which is most likely, is that F1 is CF_2, whose chemical shift in $(CF)_n$ is -111 ppm (Fig. 2 (c)). The missing of the corresponding ^{13}C signal in the 1D spectra (Figs. 4 (a) and 4 (b)) and in the 2D spectra (Figs. 5 and 10) may be attributed to broad ^{13}C linewidth expected from the broad ^{19}F signal of F1 (Fig. 3 (b)) and its

relatively small intensity (F1:F2:F3:F4 = 0.12:1.0:0.11:0.07). The broad $^{13}CF_2$ signal may be overlapped by the two envelopes of the C1 and C2 signals.

The second one is fluorine found in single-walled carbon nanotubes appearing at -120 ppm, which was ascribed to C-F with "a reduced covalent bond" [40]. As there is not much NMR data other than the ^{19}F shift for this assignment, we just pointed out here this as one possible assignment of F1. The third one is F1 being fluorine bonded to sp^2 carbon, which is invoked by noting the chemical shift of the *peri*-fluorine in 1-fluoronaphthalene being -123.85 ppm and J_{CF} = 253.4 Hz [41]. However, this is most unlikely as no ^{13}C-^{19}F *J* coupling was appreciable for F1, and the cleavage of the graphite plane upon fluorination and/or replacement of hydrogen by fluorine is necessary for creation of such a pair. Since short T_2 for F1 (and C2) may result in the failure of observing ^{13}C-^{19}F *J* coupling, we would like to mention this possibility here. To conclude, F1 is temporary assigned to CF_2 located at the edges of $C_{2.8}F$ and/or in other defected structures. Note, however, this assignment is based only on its ^{19}F chemical shift.

The results of the ^{13}C- ^{19}F dipolar and *J* correlation experiments described above for F2 are consistent with the assignment of F2 being fluorine chemically bonded to the sp^3 carbon (C2). The chemical-shift difference between C-F in $C_{2.8}F$ and that in $(CF)_n$ can be attributable to hyperconjugation involving the C-F and C-C bonds in $C_{2.8}F$. Electron donation from C-C bonds involving sp^2 carbons to the antibonding σ* orbital of C-F elongates the C-F bond length and leads to high-frequency shift of ^{19}F.

As the results of all correlation experiments are similar for F2 and F3 except for the longer C1-F3 distance, we consider that F3 also belongs to the C-F group of $C_{2.8}F$. Considering the ^{19}F chemical shift of "covalent" C-F in $(CF)_n$ appears at -182 ppm, we

may attribute the observed low-frequency shift (~30 ppm) of the ^{19}F chemical shift of F3 from that of F2 to a decrease of the hyperconjugation interaction with concomitant increase of the covalency of the C-F bonding in C-F3. The decrease of the hyperconjugation interaction is consistent with the longer C1-F3 distance. This and the close proximity between F2 and F3 indicated in Fig. 6 lead us a structural model given in the following section 4.2.

The assignment of F4 at -182 ppm being free F^- ion has already been examined above. Here, we would like to point out that the assignment is supported by the similar ^{19}F shift of a fluorine ion in ionic crystals such as NaF (-221 ppm) and MgF_2 (-187 ppm) [19]. Note that this F^- ion is different from FHF^-, whose chemical shift is -154.5 ppm in K[FHF] [42].

4.2.Structure of $C_{2.8}F$

It was postulated that, for stage-1 C_xF, the major structure containing F2 is $C_{2.0}F$ composed of the C-F group flanking the sp^2 carbon (Fig. 1 (c) and Fig. 11 (a)) [18]. The abovementioned ^{19}F-^{19}F dipolar correlation experiment suggests that a large C_xF domain is interleaved by C-F with sp^3 carbon (F3). In addition, there are the F1 sites at the sheet edges and other defections. Here we roughly evaluate the width of the interleaving C-F domain (the F3 interleaving domain).

A diffusion path length for time t is usually given by

$$\chi^2 = a\, D\, t, \qquad (2)$$

where D is the diffusion constant, and a is a proportional constant depending on the model chosen. For 1D diffusion, a is given by 4/3, and we simply assume $a = 1$ as the difference among models is not serious in the following order estimation. The spin-diffusion time t is

assumed roughly to be ca. 0.1 sec from the observed 2D ^{19}F-^{19}F exchange cross peaks for F2-F3 (Fig. 6) under MAS with ν_R = 35 kHz. As the spin-diffusion time is scaled as $1/\nu_R$ by MAS [43, 44], we estimate the spin-diffusion time for the static case to be ca. 3×10^{-3} s. The diffusion constant D for ^{19}F-^{19}F spin diffusion was ca. 7×10^{-12} cm^{2}s^{-1} for static CaF_2 [45]. Although the ^{19}F density in CaF_2 is much larger than that in $C_{2.8}F$, in other words, the spin diffusion is much faster in CaF_2, we adopted this value as for the fast limit. Then we found the mean-square diffusive path length $<\chi^2>^{1/2} \sim 1$ nm, which gives an upper-limit of the width of the F3 interleaving domain. With these, we attribute the C-F3 group to a result of fluorination of the sp^2 carbon in the stage-1 C_xF structures, which is illustrated in Fig. 11 (b). Note that this is rather a minor structure with its small relative amount as compared to F2 (F2:F3 = 1.0:0.11) determined by the ^{19}F lineshape analysis (Fig. 3(b)). Furthermore, we

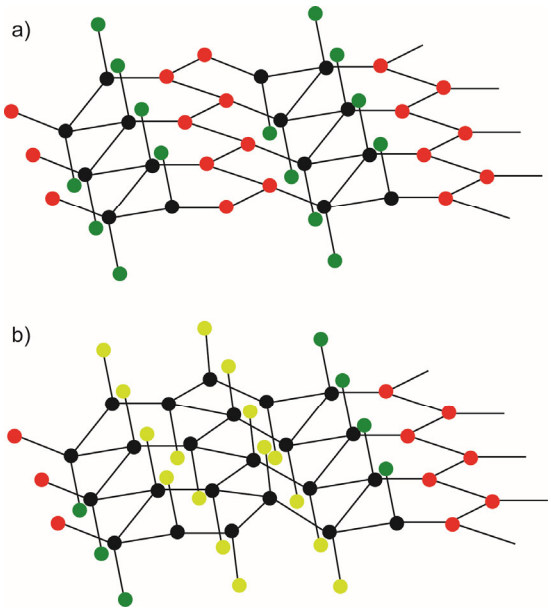

Figure 11. Schematical illustration of the $C_{2.0}F$ structure (a) with the F3 moiety (b). The black and red circles represent sp^3 and sp^2 carbons, respectively. The green and pale-green circles denote F2 and F3, respectively.

would like to mention that it is difficult to examine by NMR whether the F3 interleaving domain appears periodically or randomly in the $C_{2.8}F$ layer.

4.3. Examination of J_{CF}

In contrast to the large difference in the ^{19}F chemical shift between $C_{2.8}F$ (~ -143 ppm) and $(CF)_n$ (~ -183 ppm), the observed J_{CF} for the two compounds are similar 193 ± 4 Hz ($C_{2.8}F$) and 197 ± 7 Hz ($(CF)_n$). As have pointed out by Emsley et al. that, unlike one-bond J_{CH}, the one-bond J_{CF} is not a good indication of the hybridization of the carbon atom because the spin-orbit contribution is comparable to that of the Fermi-contact term [46]. However, it was also shown for several series of compounds that J_{CF} increases with increasing the relative amount of s-character in the carbon orbital used in bonding to fluorine [28]. As for an example of such correlation of ^{19}F shift and J_{CF}, $^{19}F/^{13}C$ chemical shift and J_{CF} values reported for six organic compounds with a series of tertiary (bridge-head) C-F groups (Fig. 12 [47, 48]), whose steric strain increases in series, are collated in Table 1. We also collated the observed values for $C_{2.8}F$ and $(CF)_n$ in Table 1 for comparison. It is notable that the three observables in (1) to (6) encompass those corresponding ones obtained for C-F in $C_{2.8}F$ and $(CF)_n$.

The observed trend of ^{19}F chemical shift for the compounds (1) to (6) was explained as follows [49]: The low-frequency shift for (1) to (3) is attributable to a decrease in σ_{CC}-σ_{CF}* (and σ_{CH}-σ_{CF}*) interactions with a concomitant decrease in the ionicity of the C-F bond. As one proceeds to the more strained system (4) to (6), the large deshielding "through-space" effect between the two bridgeheads positions suddenly appear. The similar trend is notable for ^{13}C chemical shift. These show that the ^{19}F chemical shift is prone to be affected by many effects, and the direct comparison

among ^{19}F chemical shifts for unrelated compounds is thus not quite useful for discussion of chemical bonding.

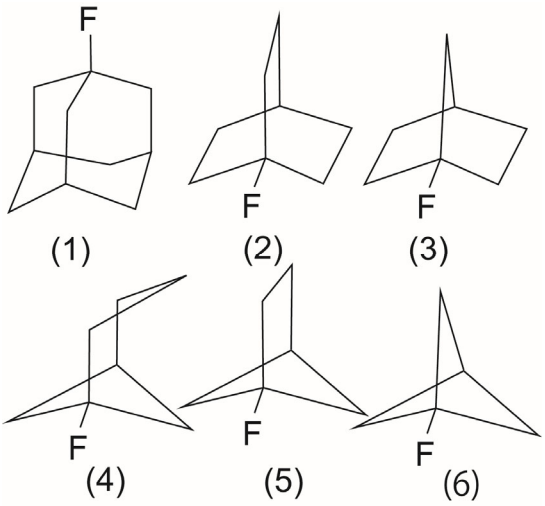

Figure 12. Molecular structures of compounds (1-6) used for comparison of NMR data in Table 1.

In contrast, the J_{CF} values show a general trend for (1) to (6); it shows progressive increase as the compounds become more strained. It was also shown that magnitude of J_{CF} in (1) to (6) displays a linear correlation with J_{CH} in the parent hydrocarbons [48]. This indicates that the J_{CF} of a bridgehead fluoride can be a good measure for the s-character of the C-F bond. It is true that the tertiary C-F bond in $C_{2.8}F$ as well as $(CF)_n$ is not exactly the "bridge-head" C-F, however, the observed J_{CF} value of 197 Hz for $(CF)_n$ and 194 Hz for $C_{2.8}F$ may indicate s-character similar to those in (2) and (3). The distortion of the tertiary C from the sp^3 tetrahedral structure in stage-1 C_xF as postulated by analysis of neutron diffraction [18] may result in increasing the J_{CF} value for $C_{2.8}F$.

Table 1. $^{19}F/^{13}C$ chemical shifts and J_{CF} values of the fluoride (1)~(6)[a] (Fig. 12) together with those obtained in this work for $C_{2.8}F$ and $(CF)_n$.

Compd.	$\delta(^{19}F)$ (ppm)	$\delta(^{13}C)$ (ppm)	$\lvert J_{CF}\rvert$ (Hz)
(1)	-127.8	90.8	185.9
(2)	-147.6	92.5	185.3
(3)	-182.0	103.8	208.1
(4)	-125.1	93.8	233.4
(5)	-157.4	95.21	257.6
(6)	-132.4	74.93	332.5
$C_{2.8}F$	-143	83.1	193
$(CF)_n$	-183	89	197

[a]For (1)~(6), the ^{19}F shifts are from Ref. [47] and the ^{13}C shifts and J_{CF} values are from Ref. [48].

Effects of the hyperconjugation interaction, which brings the high-frequency shift for ^{19}F and the elongation of the C-F bond in $C_{2.8}F$, on the J_{CF} coupling constant, should also be considered. Adcock et al. suggested from examination of some norborn-7-yl fluoride derivatives that a dislocation of the proportionality between the s-character of a C-F bond and its corresponding J_{CF} coupling may occur where σ_{CF}* is strongly perturbed by homohyperconjugation [50]. Similarly in $C_{2.8}F$, the hyperconjugation interaction between the C-F and C-C bonds involving the antibonding σ_{CF}* bond may also play a role in the coupling constant. For further examination, compilation of J_{CF} values of various graphite fluorides and application of theoretical calculation are desirable. At present, we are planning to conduct *J* experiments at lower

static magnetic fields with faster MAS frequencies with a hope of elongating ^{13}C and ^{19}F T_2 values to facilitate determination as well as to increase accuracy of the experimental J_{CF} values.

To conclude, there is no apparent NMR evidence for the so-called "semi-covalent" C-F bond being appreciably different from a "normal" or "standard" single C-F bond between a tertiary carbon and fluorine in a hydrocarbon. Further, we showed formation of another C-F bonding between sp^3 carbon and fluorine (F3) and postulated its structure.

5. Concluding Remarks

High-resolution solid-state NMR has been one of the most useful methods in the investigation of amorphous solids. In fact, solid-state NMR has been applied to examine structures of fluorinated carbon materials; some of the earlier works have been reviewed by Panich [19] and Touhara [27]. In this work, we also applied high-resolution solid-state NMR to examine local structures of a stage-1 layered carbon-fluorine compound ($C_{2.8}F$). In addition to the various 2D correlation experiments using "through space" ^{13}C-^{19}F and ^{19}F-^{19}F dipolar interactions to reveal distance proximities among ^{13}C/^{19}F spins, we used the *J* interaction in this work. A pair of spins interacts with each other by the *J* interaction if they are connected by σ bonding. Hence, the *J* interaction can be useful not only to obtain "through bond" correlation, but also to discuss covalency of a chemical bond. It is thus strange to find that so far there have been no attempts to employ the *J* interaction for structural investigation and discussion of the covalency of the so-called "semi-ionic/semi-covalent" bond in C_xF. This unpopularity may mostly be

attributable to apparent ^{13}C linewidth being much broader than the J_{CF} coupling (160~285 Hz for the direct C-F bond [28]), which obscures the *J* splitting.

To observe the J_{CF} interaction in fluorinated carbon materials, one has to remove ^{19}F-^{19}F homonuclear dipolar interaction and ^{19}F-^{13}C heteronuclear dipolar interaction without appreciably reducing the *J* interaction. Conventional ^{19}F-^{13}C dipolar decoupling, such as XiX [32], cannot be applied as it also removes the *J* interaction. It was shown by Terao et al. that the one-bond *J* coupling between ^{13}C and ^{1}H spins in adamantane can be observed by applying homonuclear ^{1}H-^{1}H decoupling and MAS [51]. In this work, removal of both ^{19}F-^{19}F homonuclear and ^{13}C-^{19}F heteronuclear dipolar interactions was done by fast MAS. The remaining ^{13}C linewidth is, however, still much broader than the *J* splitting. As the linewidth is the so-called inhomogeneous one, which is mainly attributable to distribution of local structures, one can remove it by a proper pulse sequence, such as, a Hahn echo. Indeed in this work, we showed that it is feasible to observe the one-bond J_{CF} interaction with using fast MAS and a proper pulse sequence. It is hoped that this work prompts application of NMR techniques based on the *J* interaction to various carbon/fluoride materials, leading to compilation of the J_{CF} values with deeper understanding of the nature of the C-F bond.

Acknowledgments

This work was supported by R&D Initiative for Scientific Innovation on New Generation Batteries 2 (RISING2) Project administrated by New Energy and Industrial Technology Development Organization (NEDO). The authors thank Mr. Takashi Moroishi for his support for the experiment.

Appendix A. Supplementary data

Supplementary data related to this article can be found at (a link will be given afterward).

References

[1] Watanabe N, Nakajima T, Touhara H. Graphite fluorides. Amsterdam: Elsevier; 1988.

[2] Watanabe N, Nakajima T. Graphite fluorides and carbon–fluorine compounds. Boca Raton: CRC; 1991.

[3] Rüdorff W, Rüdorff GZ. Zur Konstitution des Kohlenstoff-Monofluorids. Anorg Allg Chem 1947, 253, 281-296.

[4] Touhara H, Kadono K, Fujii Y, Watanabe N. On the structure of graphite fluoride. Z Anorg Allg Chem 1987;544:7–20.

[5] Watanabe N, Two types of graphite fluorides, $(CF)_n$ and $(C_2F)_n$, and discharge characteristics and mechanisms of electrodes of $(CF)_n$ and $(C_2F)_n$ in lithium batteries. Solid State Ionics 1980; 1: 87-110.

[6] Charlier JC, Gonze X, Michenaud JP. First-principles study of graphite monofluoride $(CF)_n$. Phys Rev B 1993; 47(24): 16162-16168.

[7] Ebert LB, Brauman JI, Huggins RA. Carbon monofluoride. Evidence for a structure containing an infinite array of cyclohexane boats. J Am Chem Soc 1974; 96: 7841-7842.

[8] Sato Y, Itoh K, Hagiwara R, Fukunaga T, Ito Y. Short-range structures of poly(dicarbon monofluoride) $(C_2F)_n$ and poly(carbon monofluoride) $(CF)_n$. Carbon 2004; 42(14) 2897–2903.

[9] Rüdorff W, Rüdorff G. Tetrakohlenstoffmonofluorid, eine neue Graphit-Fluor-Verbindung. Chem Ber 1947; 80, 413-417.

[10] Lagow RJ, Badachhape RB, Ficalora P, Wood JL, Margrave JL. A new method of preparation of tetracarbon monofluoride. Syn Inorg Metal-Org Chem 1972; 2(2) 145-149.

[11] Nakajima T, Kawaguchi M, Watanabe N. Ternary intercalation compound of graphite with aluminum fluoride and fluorine. Z Naturforsch 1981; 36b: 1419-1423.

[12] Mallouk T, Bartlett N. Reversible intercalation of graphite by fluorine: a new bifluoride, $C_{12}HF_2$, and graphite fluorides, C_xF ($5 > x > 2$). J Chem Soc Chem Commun 1983:103–5.

[13] Mallouk T, Hawkins BL, Conrad MP, Zilm K, Maciel GE, Bartlett N. Raman, infrared and NMR studies of the graphite hydrofluorides $C_xF_{1-\delta}(HF)_\delta$. Philos Trans R Soc London 1985;.A314:.179–87.

[14] Palchan I, Davidov D, Selig H. Preparation and properties of new graphite–fluorine intercalation compounds. J Chem Soc Chem Commun 1983: 657-658.

[15] Sato Y, Kume T, Hagiwara R, Ito Y. Reversible intercalation of HF in fluorine–GICs. Carbon 2003; 41(2): 351–7.

[16] Hamwi, A. Fluorine reactivity with graphite and fullerenes. fluoride derivatives and some practical electrochemical applications. J Phys Chem Solids 1996; 57(6-8): 677-688.

[17] Hamwi A, Daoud M, Cousseins, JC. Graphite fluorides prepared at room temperature. 1. Synthesis and characterization. Synth Met 1988; 26: 89−98.

[18] Sato Y, Itoh K, Hagiwara R, Fukunaga T, Ito Y. On the so-called "semi-ionic" C–F bond character in fluorine–GIC. Carbon 2004; 42:3243-3249.

[19] As for a review of NMR studies, see: Panich, AM. Nuclear magnetic resonance study of fluorine–graphite intercalation compounds and graphite fluorides. Synth Metals 1999; 100: 169-185.

[20] Giraudet J, Dubois M, Guérin K, Delabarre C, Hamwi A, Masin F. Solid-state NMR study of the post-fluorination of $(C_{2.5}F)_n$ fluorine-GIC. J Phys Chem 2007; B111 (51), 14143-14151.

[21] Okazaki K, Uchimoto Y, Abe T, Ogumi Z. Charge−discharge behavior of bismuth in a liquid electrolyte for rechargeable batteries based on a fluoride shuttle. ACS Energy Lett 2017; 2: 1460-1464.

[22] Reddy MA. Fichtner M. Batteries based on fluoride shuttle. J Mater Chem 2011; 21: 17059-17062.

[23] Hamwi A, Guérin K, Dubois M. Fluorine-intercalated graphite for lithium battery in Fluorinated materials for energy conversion; Nakajima, T., Groult, H., Eds.; Elsevier: Amsterdam, 2005; Chapter 17.

[24] Hagiwara R, Lerner M, Bartlett N, Nakajima T. A lithium/C_2F primary battery. J Electrochem Soc. 1988; 135(9): 2393-2394.

[25] Kouvetakis J, Sasaki T, Shen C, Hagiwara R, Lerner M, Krishnan KM, Bartlett N. Novel aspects of graphite intercalation by fluorine and fluorides and new B/C, C/N and B/C/N materials based on the graphite network. Synthetic Metals, 1990; 34: 1-7.

[26] Suganuma S, Mizu T, Sakagoshi H, Momota K, Okino F, Touhara H. Fluoride Ion Conduction of Fluorine Intercalated Graphite C_xF. Tanso 1993; 160: 266-271.

[27] As for a review, see: Tokuhara H. Okino F. Property control of carbon materials by fluorination. Carbon 2000; 38: 241-267.

[28] Dolbier Jr RD. Guide to fluorine NMR for organic chemists, 2nd ed. Wiley; 2016.

[29] Groß U, Rudiger S, Grimmer AR, Kemnitz E. ^{19}F-NMR solid state investigations of monovalent alkali metal fluorides and tetra-alkylammonium fluorides. J Fluorine Chem 2002; 115 (2): 193-199 and references therein.

[30] Bielecki A, Brum DP. Temperature dependence of ^{207}Pb MAS spectra of solid lead nitrate. An accurate, sensitive thermometer for variable-temperature MAS. J Magn Reson 1995; A116 (2): 215-220.

[31] Sardashti M, Maciel GE. Effects of sample spinning on cross polarization. J Magn Reson 1987; 72 (3): 467-474.

[32] Detken A, Hardy EH, Ernst M, Meier BH. Simple and efficient decoupling in magic-angle spinning solid-state NMR: the XiX scheme. Chem Phys Lett 2002; 356 (3-4): 298-304.

[33] Oas TG, Griffin RG, Levitt MH. Rotary resonance recoupling of dipolar interactions in solid-state nuclear magnetic resonance spectroscoopy. J Chem Phys 1988; 89 (2): 692-695.

[34] Ernst RR, Bodenhausen G, Wokaun A. Principles of nuclear magnetic resonance in one and two dimensions. Oxford, 1987.

[35] Sakellariou D, Lesage A, Emsley L. Spectral editing in solid-state NMR using scalar multiple quantum filters. J Magn Reson 2001; 151: 40-47.

[36] Coelho C, Azais T, Bonhomme-Coury L, Maquet J, Massiot D, Bonhomme C. Application of the MAS-J-HMQC experiment to a new pair of nuclei {^{29}Si,^{31}P}: $Si_5O(PO_4)_6$ and SiP_2O_7 polymorphs. J Magn Reson 2006; 179: 114-119.

[37] Giraudet J, Dubois M, Hamwi A, Stone WEE, Pirotte P, Masin F. Solid-State NMR (^{19}F and ^{13}C) study of graphite monofluoride $(CF)_n$: ^{19}F spin-lattice magnetic relaxation and ^{19}F/^{13}C distance determination by Hartmann-Hahn cross polarization. J Phys Chem B 2005; 109: 175-181.

[38] Krawietz TR, Haw JF. Characterization of poly(carbon monofluoride) by ^{19}F and ^{19}F to ^{13}C cross polarization MAS NMR spectroscopy. Chem. Commun 1998; 19: 2151-2152

[39] van Rossum B-J, de Groot CP, Ladizhansky V, Vega S, de Groot HJM. A method for measuring heteronuclear (^{1}H-^{13}C) distances in high speed MAS NMR. J Am Chem Soc 2000; 122 (14):3465-3472.

[40] Claves D, Li H, Dubois M, Ksari Y. An unusual weak bonding mode of fluorine to single-walled carbon nanotubes. Carbon 2009; 47:2557-2562.

[41] Gribble GW, Keavy DJ, Olson ER, Rae ID, Staffa A, Herr TE, et al. Fluorine Deshielding in the Proximity of a Methyl Group. An Experimental and Theoretical Study, Magn Reson Chem 1991; 29: 422-432.

[42] Delabarre C, Guérin K, Dubois M, Giraudet J, Fawal Z, Hamwi A. Highly fluorinated graphite prepared from graphite fluoride formed using BF3 catalyst. J Fluorine Chem 2005. 126: 1078-1087.

[43] Kubo A. McDowell CA. Spectral spin diffusion in polycrystalline solids under magic-angle spinning. J Chem Soc Faraday Trans 1 1988; 84(11): 3713-3730.

[44] Zhang S. Meier BH. Ernst RR. Local monitoring of proton spin diffusion in static and rotating samples via spy detection. Solid State Nucl Magn Reson 1992; 1: 313-320.

[45] Zhang W. Cory DG. First direct measurement of the spin diffusion rate in a homogeneous solid. Phys Rev Lett 1998; 80(6): 1324-1327.

[46] Emsley JW, Phillip L, Wray V. Fluorine coupling constants. Prog in Nucl Magn reson Spectrsc 1976; 10 (3/4): 83-756.

[47] Bradshaw TK, Hine PT, Della EW. ^{19}F Chemical shifts of bridgehead fluorides. Org Magn Reson 1982; 16 (1); 26-27.

[48] Della EW, Cotsaris E, Hine PT. Synthesis and carbon-13 nuclear magnetic resonance studies of some bridgehead fluorides: Carbon-fluorine coupling constants. J Am Chem Soc 1981; 103 (14): 4131-4135.

[49] Adcock W, Abeywickrema AN, Kok GB. Transmission of polar substituent effects in bicycloalkane systems. Synthesis and nuclear magnetic resonance study (carbon-13 and fluorine-19) of 4-substituted bicyclo[2.2.l]hept-l-y1 fluorides. J Org Chem 1984; 49 (8): 1387-1397.

[50] Adcock W, Angus DI, Lowe DA. ^{19}F and ^{13}C NMR study of some norborn-7-yl fluoride derivatives. Magn Reson Chem 1996; 34: 675-680.

[51] Terao T. Miura H. Saika A. High-resolution J-resolved NMR spectra of dilute spins in solids. J. Chem. Phys. 1981; 75(3): 1573-1574.